Nanoscale

PAPER

View Article Online
View Journal | View Issue

Cite this: *Nanoscale*, 2018, **10**, 6099

A C_{20} fullerene-based sheet with ultrahigh thermal conductivity†

Yupeng Shen, [a] Fancy Qian Wang,[a] Jie Liu, [a] Yaguang Guo,[a] Xiaoyin Li,[a] Guangzhao Qin, [b] Ming Hu [b] and Qian Wang *[a]

Received 5th January 2018,
Accepted 20th February 2018

DOI: 10.1039/c8nr00110c

rsc.li/nanoscale

A new two-dimensional (2D) carbon allotrope, Hexa-C_{20}, composed of C_{20} fullerene is proposed. State-of-the-art first principles calculations combined with solving the linearized phonon Boltzmann transport equation confirm that the new carbon structure is not only dynamically and thermally stable, but also can withstand temperatures as high as 1500 K. Hexa-C_{20} possesses a quasi-direct band gap of 3.28 eV, close to that of bulk ZnO and GaN. The intrinsic lattice thermal conductivity κ_{lat} of Hexa-C_{20} is 1132 W m^{-1} K^{-1} at room temperature, which is much larger than those of most carbon materials such as graphyne (82.3 W m^{-1} K^{-1}) and penta-graphene (533 W m^{-1} K^{-1}). Further analysis of its phonons uncovers that the main contribution to κ_{lat} is from the three-phonon scattering, while the three acoustic branches are the main heat carriers, and strongly coupled with optical phonon branches *via* an absorption process. The ultrahigh lattice thermal conductivity and an intrinsic wide band gap make the Hexa-C_{20} sheet attractive for potential thermal management applications.

Introduction

The successful synthesis of C_{60} [1] fullerenes has attracted extensive attention because of their fantastic graphitic cage structures and great potential in technological applications.[2–5] Among the family of fullerenes, the smallest member, C_{20} cage, is particularly interesting because of its unique atomic configuration. It is composed of only 12 pentagons, violating the "isolated pentagon rule"[6,7] in fullerene science. Although the cage structure is not the lowest energy configuration of C_{20} due to its high curvature and strong strain,[8] it is dynamically stable and has already been successfully synthesized in 2000.[9] C_{20} fullerene also exhibits exceptional properties. For instance, the electron–phonon coupling of fullerene cages increases with the curvature, and thus C_{20} fullerene was predicted to be a promising unit for high-temperature superconducting materials.[10] In addition, C_{20} fullerene shows magnetization discontinuities when an external magnetic field is applied.[11] These novel properties have encouraged the study of using C_{20} fullerene as a building block to construct C_{20}-based crystals. Different from the conventional materials where atoms are the building blocks, for the cage assembled materials, the phonon spectra are susceptible to significant changes due to the coupling of intra-cluster and inter-cluster vibrations, which may influence the thermal conductivity. In the past two decades, materials composed of C_{20} fullerene are widely studied, including one- and three-dimensional structures.[12–15] However, C_{20} fullerene-based 2D structures have not been well explored especially for their thermal conductivity, which motivates us to carry out this study.

On the other hand, the carbon structures show diverse lattice thermal conductivities (κ_{lat}) due to the flexible hybridization of carbon atoms. For instance, the room temperature κ_{lat} of carbon allotropes spans a large range from the lowest value of about 0.01 W m^{-1} K^{-1} in amorphous carbon to the highest one of 3000–5800 W m^{-1} K^{-1} in graphene and carbon nanotubes,[16] while the κ_{lat} of C_{60} and its assembled FCC solids have been reported to be 0.2–0.7 W m^{-1} K^{-1}.[17–19] Therefore, it is interesting to study the phonon transport properties of C_{20} fullerene-based structures.

In this work, we propose a new 2D carbon allotrope, named Hexa-C_{20}, from assembling the C_{20} cages by sharing pentagonal faces, and systematically study its stability, electronic structure, and lattice thermal conductivity.

Computational methods

The atomic structure of the Hexa-C_{20} sheet is optimized and its electronic band structure is calculated using the density

[a]*Center for Applied Physics and Technology, Department of Materials Science and Engineering, HEDPS, BKL-MEMD, College of Engineering, Peking University, Beijing 100871, China. E-mail: qianwang2@pku.edu.cn*
[b]*Institute of Mineral Engineering, Division of Materials Science and Engineering, RWTH Aachen University, 52064 Aachen, Germany*

†Electronic supplementary information (ESI) available. See DOI: 10.1039/c8nr00110c

functional theory (DFT) and the projector augmented wave (PAW)[20] method as implemented in the Vienna *Ab initio* Simulation Package (VASP).[21] The Perdew–Burke–Ernzerhof (PBE) exchange–correlation functional within the generalized gradient approximation (GGA)[22] is employed to treat the electronic exchange–correlation interaction. For geometry relaxation, the convergence thresholds for the total energy and force component are set to 10^{-6} eV and 10^{-4} eV Å^{-1}, respectively. To obtain an accurate band gap, we also recalculate the electronic structure by using the Heyd–Scuseria–Ernzerhof (HSE06)[23,24] functional. The energy cutoff for wave functions is set to 500 eV, while the Brillouin zone is represented by k points with a grid density of $2\pi \times 0.02$ Å^{-1} in the reciprocal space using the Monkhorst–Pack scheme. A vacuum space of 16 Å in the direction perpendicular to the sheet is used to make the two-dimensional (2D) structure free of the interactions with its periodic images.

The microscopy description of κ_{lat} can be derived from the phonon Boltzmann transport equation (BTE)[25] within the three-phonon scattering framework. The intrinsic κ_{lat} of an infinite and isotropic single-layer can be expressed as:

$$\kappa_{lat}^{\alpha} = \frac{1}{k_B T^2 V N^2} \sum_{\lambda} f_{\lambda}(f_{\lambda}+1)(\hbar\omega_{\lambda})^2 \nu_{\lambda}^{\alpha}\nu_{\lambda}^{\alpha}\tau_{\lambda}$$

where ω_λ and τ_λ are the frequency and phonon lifetime of each phonon mode λ, respectively. ν_λ^α is the group velocity along the thermal transport direction α. k_B, f and $\hbar$ are the Boltzmann constant, the Bose distribution function and the reduced Planck constant. And N and V are the number of uniformly spaced q points in the Brillouin zone and the volume of the unit cell, respectively. Herein, the layer thickness is taken as 7.14 Å, which is the optimized interlayer spacing of the double layer structure of Hexa-C_{20}. We calculate the phonon relaxation time τ_λ using an iterative approach, as implemented in the ShengBTE package.[26] As needed for the input, the harmonic and anharmonic interatomic force constants (IFCs) are calculated using a $3 \times 3 \times 1$ supercell, which are obtained from DFT calculations performed in VASP. Besides, the cutoff radius is set to the 6th nearest neighbors and the scalebroad parameter is selected as 0.1 to ensure the accuracy of our calculations.

Results and discussion

Structure and electronic properties

Based on the building block, C_{20} cage, we construct a new 2D fullerene-based sheet, named Hexa-C_{20}, by assembling six C_{20} cages through face sharing. The optimized geometry is plotted in Fig. 1(a) and (b), where one hexagon is formed to release the resulting strain for better stability. There are 34 atoms in a unit cell, and the optimized lattice constants are $a = b = 6.96$ Å. A large buckling of 3.62 Å is observed upon structural optimization. The space group of Hexa-C_{20} belongs to $P6/mmm$ (191).

We then examine the stability of Hexa-C_{20}, including its thermodynamic, dynamic, thermal and mechanical stability. We first perform total energy calculations to investigate the thermodynamic stability of Hexa-C_{20}. The results are presented in Fig. 2a. Although Hexa-C_{20} is metastable compared with gra-

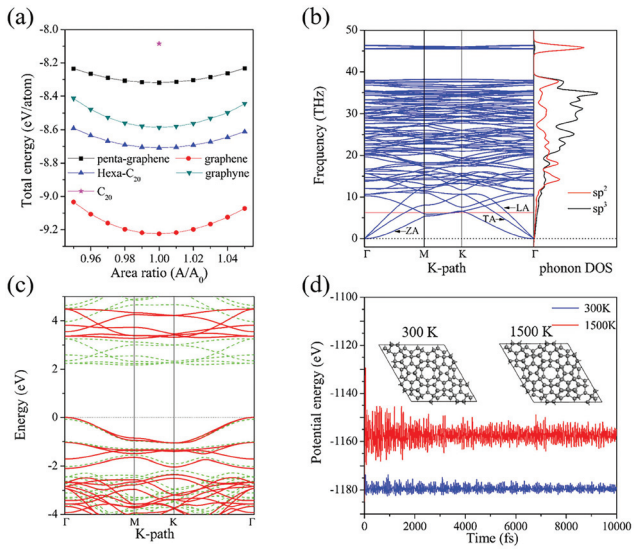

Fig. 2 (a) Area dependence of total energy per atom for some 2D carbon allotropes. (b) Calculated phonon dispersion and phonon DOS, and (c) electronic band structure of Hexa-C_{20}. (d) Total potential energy fluctuation during AIMD simulation at 300 K (blue solid line) and 1500 K (red solid line). The insets show the atomic configurations at the end of AIMD simulations at 300 K and 1500 K, respectively.

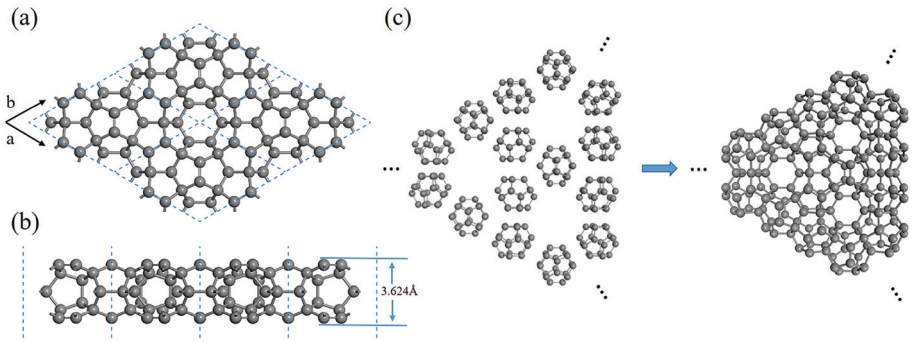

Fig. 1 (a) Top and (b) side views of the optimized structure of Hexa-C_{20}, displayed in a $2 \times 2 \times 1$ supercell. (c) The assembling process from the C_{20} cage to the Hexa-C_{20} sheet by face-sharing.

phene, it is energetically favorable over graphyne, which was successfully synthesized in experiment.[27] Besides, the binding energy of the Hexa-C_{20} sheet is −8.71 eV per atom, which is lower than that of −8.32 eV per atom of penta-graphene[28] and that of −8.08 eV per atom for an isolated C_{20} cage, because using the hexagons as the linkages of Hexa-C_{20} partially releases the strain.

To examine the dynamic stability of Hexa-C_{20}, we calculate its phonon dispersion and phonon density of states by using the PHONOPY package,[29] as shown in Fig. 2b. The absence of imaginary modes in the entire Brillouin zone confirms its dynamic stability. We note that the three acoustic branches, including the in-plane transverse acoustic (TA) mode, longitudinal acoustic (LA) mode, and the out-of-plane flexural (ZA) acoustic mode, are much more dispersive compared to those optical branches. However, several low-lying optical branches are strongly coupled with the three acoustic branches, indicating that the optical branches also make contributions to the lattice thermal conductivity. Besides, we also observe a significant phonon gap between 38 THz and 45 THz. The detailed analysis of the phonon density of states reveals that the contributions from the sp^2 hybridized carbon atoms are predominant in the high frequency regions, which is similar to some other 2D carbon allotropes.[30,31]

To further study the thermal stability of Hexa-C_{20}, we perform *ab initio* molecular dynamics (AIMD) simulations at 300 K by using the canonical (NVT) ensemble.[32] A 2 × 2 × 1 supercell is constructed to simulate the 2D sheet for reducing the constraint of periodic boundary conditions and exploring possible structure reconstruction. The results are shown in Fig. 2d. After heating for 10 ps with a time step of 1 fs at 300 K, the total potential energy remains almost constant while the geometry of Hexa-C_{20} remains nearly intact without apparent distortion, suggesting that the structure is thermally stable at 300 K. Furthermore, we find that the Hexa-C_{20} sheet can even withstand temperatures as high as 1500 K, providing a large work temperature range due to its high bond strength.

Besides the thermodynamic and thermal stability discussed above, we also need to study the mechanical stability which requires that the strain energy should be positive-definiteness with the lattice distortion. We therefore calculate the linear elastic constants by using the finite distortion method implemented in VASP. For a mechanically stable 2D sheet with a hexagonal lattice, the elastic constants should obey the Born–Huang criteria:[33] $C_{11} > C_{12}$, $C_{44} > 0$ and $(C_{11} + C_{12})C_{33} > 2C_{13}$.[2] Our calculated elastic constants are listed in Table S1,† which meet these criteria, thus confirming the mechanical stability of Hexa-C_{20}.

Based on the structure of Hexa-C_{20}, we study its electronic band structure, as plotted in Fig. 2c. The valence band maximum (VBM) and conduction band minimum (CBM) are located on the Γ point and M point, respectively, while the second conduction band with energy 0.1 eV lower than the CBM locates on the Γ point, resulting in a quasi-direct band gap of 2.25 eV at the GGA-PBE level and 3.28 eV at the HSE06 level, which is comparable to those of conventional semiconductors, such as ZnO and GaN.[34,35]

Lattice thermal conductivity

Lattice thermal conductivity is an important physical property used to assess the ability of materials to conduct heat. Materials with high thermal conductivity κ_{lat} are required in cooling devices for passive heat spreading, while low thermal conductivity are desired for good thermoelectric applications. The in-plane lattice thermal conductivity of Hexa-C_{20} is calculated as a function of temperature by solving the linearized phonon Boltzmann transport equation (BTE),[36,37] as shown in Fig. 3a. The calculated thermal conductivity κ_{lat} at room temperature (300 K) is 1132 W m^{-1} K^{-1}, which is much larger than that of many carbon allotropes, such as penta-graphene[38–40] and graphyne,[41,42] demonstrating its great potential in thermal devices. We fit the κ_{lat}–T curve and find that κ_{lat} is approximately proportional to $1/T^{14.0}$, which indicates that the three-phonon scattering dominates the thermal transport. This is further confirmed by comparing the scattering rates of three-phonon scattering with the isotopic scattering process as shown in Fig. S1 in the ESI,† which indicates that the scattering rates of the three-phonon scattering are nearly ten times larger than those of isotopic scattering, suggesting that the three-phonon scattering is predominant at room temperature.

The three-phonon scattering process includes the absorption process and emission process, the former corresponds to one phonon with the combined energy of two incident phonons, while the latter refers to one incident phonon splitting into two phonons. To distinguish these two processes, we plot their scattering rates in Fig. 3b, which indicates that in the low frequency region (below 25 THz), the absorption process plays a leading role, while in the high frequency region, the emission process becomes predominant. Moreover, the normal (N) scattering rates and Umklapp (U) scattering rates are also calculated and shown in Fig. 3c. One can see that the scattering rates of the N process and U process have the same order of magnitude in the low frequency region, while the U process becomes significant when above 25 THz.

For the three-phonon scattering process, it is important to know how many scattering channels are accessible for phonons to be scattered. Such possibility is determined by the three phonon phase space P_3, which contains the scattering events that satisfy energy and momentum conservation conditions, and thus can be used to assess quantitatively the number of scattering channels.[26,43] The three phonon phase space P_3 usually inverses to κ_{lat}, which is entirely determined by the phonon dispersion of materials. The phase space available for the three-phonon process including both the N and U processes is defined as $P_3 = \frac{2}{3\Omega}\left(P_3^{+} + \frac{1}{2}P_3^{-}\right)$, where:

$$P_3^{\pm} = \sum_j \int \mathrm{d}\vec{q} D_j^{\pm}(\vec{q});$$

$$D_j^{\pm}(\vec{q}) = \sum_{jj'} \int \mathrm{d}\vec{q}' \delta\left[\omega_j(\vec{q}) \pm \omega_{j'}(\vec{q}') - \omega_{j''}\left(\vec{q} \pm \vec{q}'' - G\right)\right];$$

where $D_j^{\pm}(\vec{q})$ corresponds to the absorption (+) and emission process (−), respectively. The calculated P_3 is 1.018 × 10^{-3},

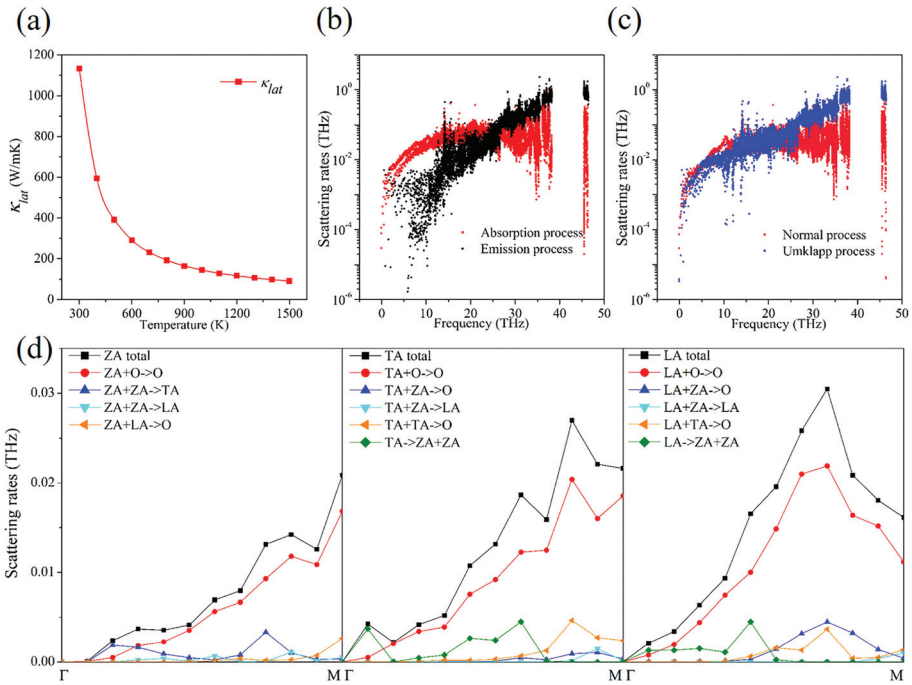

Fig. 3 (a) Variation of κ_{lat} with temperature in Hexa-C_{20}. The mode-level scattering rate decomposed into (b) absorption and emission processes, and (c) normal and Umklapp processes. (d) The main scattering channels for ZA, TA and LA phonon branches along the Γ–M direction (in-plane direction).

which is smaller than that of penta-graphene (1.38×10^{-3}), suggesting a restricted phase space in Hexa-C_{20}, and thus a larger κ_{lat} as compared to that of penta-graphene, while another key factor for phonon scattering is the intensity of every scattering channel, which depends on the anharmonicity of the phonon mode.[44,45] So we calculate the scattering rates of scattering channels along the Γ–M direction (in-plane direction) and identify the main scattering channels for ZA, TA and LA modes, as shown in Fig. 3d. Interestingly, we find that all of the three acoustic branches are mainly scattered by optical branches, indicating the strong coupling between the optical branches and the acoustic branches. Besides, we can see that due to the low frequency, the ZA mode mainly participates in the absorption process: ZA + O/ZA/LA → O/TA/LA; for the TA mode the corresponding scattering processes are: TA + O/ZA/TA → O/LA and TA → ZA + ZA, while for the LA mode the scattering includes LA + O/ZA/TA → O/LA and LA → ZA + ZA.

For more detailed information, we analyze the Debye temperature Θ of Hexa-C_{20}, which is defined as $\Theta = \frac{h\nu_m}{k_B}$, where h is Planck's constant, ν_m is the highest frequency of each corresponding phonon branch, and k_B is the Boltzmann constant. The Debye temperature Θ is a characteristic temperature above which the corresponding mode begins to excite and below which the modes are frozen out. When the Debye temperature Θ reaches 300 K, the frequency corresponds to 6.25 THz, marked as a red line in phonon dispersion in Fig. 2b. We can see that the three acoustic branches and the low-lying optical branch are partially excited at 300 K, which is quite different from the situations in graphene and penta-graphene.[38] The strong coupling between the acoustic branches and the low-lying optical branch makes the Umklapp scattering process stronger than the normal scattering process even at room temperature, resulting in the dominant contribution to the thermal transport. To further study the main heat carriers in Hexa-C_{20}, the normalized cumulative κ_{lat} as a function of frequency is calculated, as shown in Fig. 4a. We can see that phonons with frequency lower than 10 THz contribute almost 90% to thermal conductivity, which demonstrates that the three acoustic branches combined with some low-lying optical branches carry the majority of heat in Hexa-C_{20}, which is in contrast to that of graphene and penta-graphene where only the acoustic branches play predominant roles. The reason is also attributed to the lower Debye temperatures of those low-lying optical modes. Thus we focus on these branches with frequency lower than 10 THz in the following discussion.

To gain more information about the contributions of different phonon branches to the thermal conductivity, we plot the percentage contributions of three acoustic (ZA, LA and TA) and optical phonon branches as a function of temperature, as shown in Fig. 4b. At room temperature, the three acoustic branches contribute about 31% (ZA), 23% (TA) and 32% (LA) to the overall κ_{lat}, respectively. However, at the elevated temperature, phonon branches exhibit quite different behaviors: the contributions of optical phonon branches increase significantly, and converge to about 25% at 1300 K, while the contributions

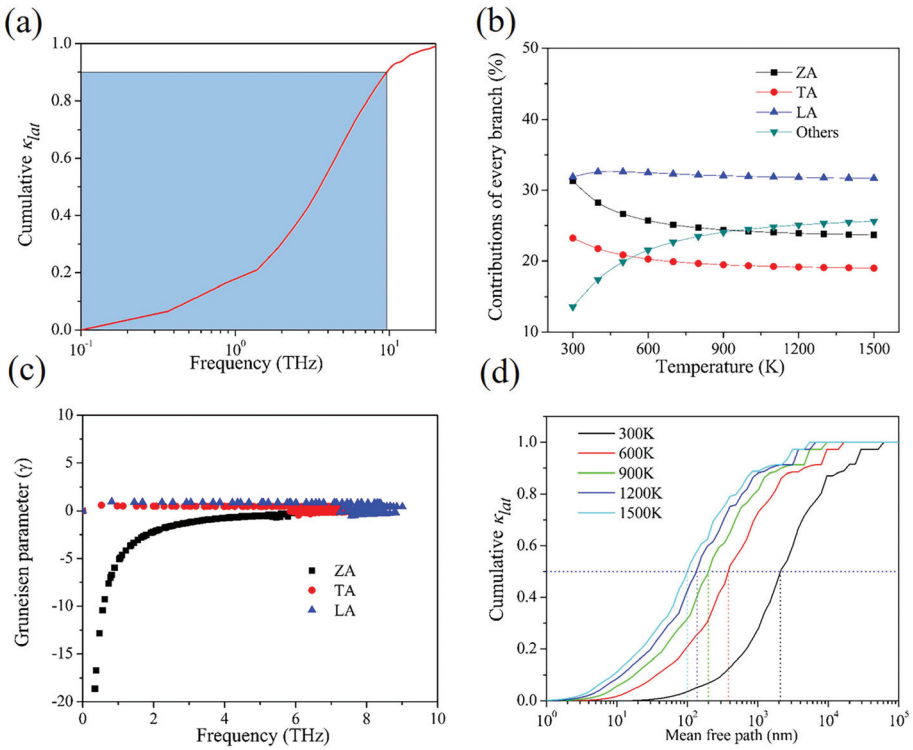

Fig. 4 (a) Normalized cumulative κ_{lat} as a function of frequency for Hexa-C_{20}. (b) Percentage contributions of the acoustic branches (ZA, LA, and TA) and the optical branches as a function of temperature. (c) Variations of Grüneisen parameter (γ) with frequency for the acoustic branches (ZA, LA, and TA). (d) Normalized κ_{lat} accumulation as a function of the phonon mean free path of Hexa-C_{20} at different temperatures, where the vertical dotted lines indicate the phonon MFPs corresponding to 50% accumulation.

of the LA mode remain constant, and the contributions of the ZA and TA modes decrease almost in the same percentage.

To further understand the above results, we calculate the mode Grüneisen parameter (γ), which is used to quantify the anharmonic interactions between phonon branches by using the quasi-harmonic approximation method. γ is defined as $\gamma = \frac{A}{\omega_\lambda}\frac{\partial\omega_\lambda}{\partial A}$, where A and ω_λ are the volume of the unit cell and angular frequency, respectively. The results are plotted in Fig. 4c. γ_{TA} (−0.45–0.59) and γ_{LA} (−0.52–0.96) show rather localized behaviors, while γ_{ZA} is divergent near the Γ point. Particularly, the γ of the ZA mode possesses much larger negative values than those of the LA and TA modes, which is a ubiquitous characteristic in 2D systems.[38,46,47] The smaller γ of acoustic branches also verifies the weak anharmonicity between the carbon atoms in this structure. Meanwhile, we also examine the cumulative thermal conductivity with respect to the allowed phonon maximum mean free path (MFP) at different temperatures to study the size dependence of κ_{lat}. The results are plotted in Fig. 4d. The total accumulation keeps increasing as MFPs increase, until reaching the plateau after MFPs increase to 61 360, 16 681, 9545, 6579 and 5426 nm, respectively. Meanwhile, the MFPs corresponding to the 50% accumulation at 300, 600, 900, 1200 and 1500 K are calculated to be 2081, 380, 198, 138 and 100 nm, respectively, proving useful information for experiment.

Conclusions

In summary, extensive studies are performed on a C_{20} fullerene-based 2D sheet (Hexa-C_{20}) by focusing on the stability, electronic structure and thermal conductivity using the state-of-the-art theoretical calculations combined with solving the linearized phonon Boltzmann transport equation. The results show that the Hexa-C_{20} sheet is a semiconductor with a band gap of 3.28 eV, and displays an ultrahigh thermal conductivity of 1132 W m^{-1} K^{-1} at room temperature. Further analysis of its phonons shows that the three-phonon scattering is predominant in thermal transport and the three acoustic branches ZA, LA and TA are the main heat carriers. This study sheds light on the design of new 2D carbon materials by using fullerene cages as the building blocks that go beyond the conventional C-atom based sheets, displaying varieties in geometry and novelties in properties.

Conflicts of interest

There are no conflicts of interest to declare.

Acknowledgements

This work is supported by grants from the National Key Research and Development Program of China (Grant No.

2016YFE0127300 and 2017YFA0205003), the National Natural Science Foundation of China (NSFC-51471004, and NSFC-21773004), and the High Performance Computing Platform of Peking University, China.

References

1 H. W. Kroto, J. R. Heath, S. C. O'Brien, R. F. Curl and R. E. Smalley, *Nature*, 1985, **318**, 162–163.
2 J. Y. Kim and J. C. Grossman, *Nano Lett.*, 2016, **16**, 4203–4209.
3 M. Sumino, K. Harada, M. Ikeda, S. Tanaka, K. Miyazaki and C. Adachi, *Appl. Phys. Lett.*, 2011, **99**, 188.
4 A. Hebard, M. Rosseinsky, R. Haddon, D. Murphy, S. Glarum, T. Palstra, A. Ramirez and A. Kortan, *Nature*, 1991, **350**, 600–601.
5 N. S. Sariciftci, L. Smilowitz, A. J. Heeger and F. Wudl, *Science*, 1992, **258**, 1474–1476.
6 H. Kroto, *Nature*, 1987, **329**, 529–531.
7 T. Schmalz, W. A. Seitz, D. J. Klein and G. Hite, *J. Am. Chem. Soc.*, 1988, **110**, 1113–1127.
8 J. C. Grossman, L. Mitas and K. Raghavachari, *Phys. Rev. Lett.*, 1995, **75**, 3870.
9 H. Prinzbach, A. Weiler, P. Landenberger, F. Wahl, J. Wörth, L. T. Scott, M. Gelmont, D. Olevano and B. V. Issendorff, *Nature*, 2000, **407**, 60–63.
10 A. Devos and M. Lannoo, *Phys. Rev. B: Condens. Matter Mater. Phys.*, 1998, **58**, 8236.
11 N. Konstantinidis, *Phys. Rev. B: Condens. Matter Mater. Phys.*, 2007, **76**, 104434.
12 S. Okada, Y. Miyamoto and M. Saito, *Phys. Rev. B: Condens. Matter Mater. Phys.*, 2001, **64**, 245405.
13 I. Spagnolatti, M. Bernasconi and G. Benedek, *Europhys. Lett.*, 2002, **59**, 572.
14 Z. Wang, X. Ke, Z. Zhu, F. Zhu, M. Ruan, H. Chen, R. Huang and L. Zheng, *Phys. Lett. A*, 2001, **280**, 351–356.
15 Z. Chen, T. Heine, H. Jiao, A. Hirsch, W. Thiel and P. V. R. Schleyer, *Chem. – Eur. J.*, 2004, **10**, 963–970.
16 A. A. Balandin, *Nat. Mater.*, 2011, **10**, 569–581.
17 J. Y. Kim and J. C. Grossman, *Nano Lett.*, 2016, **16**, 4203–4209.
18 R. Yu, N. Tea, M. Salamon, D. Lorents and R. Malhotra, *Phys. Rev. Lett.*, 1992, **68**, 2050.
19 A. Giri and P. E. Hopkins, *J. Phys. Chem. Lett.*, 2017, **8**, 2153–2157.
20 P. E. Blöchl, *Phys. Rev. B: Condens. Matter Mater. Phys.*, 1994, **50**, 17953–17979.
21 G. Kresse and J. Furthmüller, *Phys. Rev. B: Condens. Matter Mater. Phys.*, 1996, **54**, 11169.
22 J. P. Perdew, K. Burke and M. Ernzerhof, *Phys. Rev. Lett.*, 1996, **77**, 3865.
23 J. Heyd, G. E. Scuseria and M. Ernzerhof, *J. Chem. Phys.*, 2003, **118**, 8207–8215.
24 J. Heyd, G. E. Scuseria and M. Ernzerhof, *J. Chem. Phys.*, 2006, **124**, 219906.
25 M. Omini and A. Sparavigna, *Phys. B*, 1995, **212**, 101–112.
26 W. Li, J. Carrete, N. A. Katcho and N. Mingo, *Comput. Phys. Commun.*, 2014, **185**, 1747–1758.
27 Y. Li, L. Xu, H. Liu and Y. Li, *Chem. Soc. Rev.*, 2014, **43**, 2572–2586.
28 S. Zhang, J. Zhou, Q. Wang, X. Chen, Y. Kawazoe and P. Jena, *Proc. Natl. Acad. Sci. U. S. A.*, 2015, **112**, 2372–2377.
29 A. Togo, F. Oba and I. Tanaka, *Phys. Rev. B: Condens. Matter Mater. Phys.*, 2008, **78**, 134106.
30 M. J. Bucknum and R. Hoffmann, *J. Am. Chem. Soc.*, 1994, **116**, 11456–11464.
31 S. Zhang, Q. Wang, X. Chen and P. Jena, *Proc. Natl. Acad. Sci. U. S. A.*, 2013, **110**, 18809–18813.
32 S. Nosé, *J. Chem. Phys.*, 1984, **81**, 511–519.
33 F. Mouhat and F.-X. Coudert, *Phys. Rev. B: Condens. Matter Mater. Phys.*, 2014, **90**, 224104.
34 V. Srikant and D. R. Clarke, *J. Appl. Phys.*, 1998, **83**, 5447–5451.
35 M. E. Levinshtein, S. L. Rumyantsev and M. S. Shur, *Properties of Advanced Semiconductor Materials: GaN, AlN, InN, BN, SiC, SiGe*, John Wiley & Sons, 2001.
36 J. Callaway, *Phys. Rev.*, 1959, **113**, 1046–1051.
37 J. M. Ziman, *Electrons and phonons: the theory of transport phenomena in solids*, Oxford university press, 1960.
38 F. Q. Wang, J. Yu, Q. Wang, Y. Kawazoe and P. Jena, *Carbon*, 2016, **105**, 424–429.
39 H. Liu, G. Qin, Y. Lin and M. Hu, *Nano Lett.*, 2016, **16**, 3831–3842.
40 F. Q. Wang, J. Liu, X. Li, Q. Wang and Y. Kawazoe, *Appl. Phys. Lett.*, 2017, **111**, 192102.
41 X. Tan, H. Shao, T. Hu, G. Liu, J. Jiang and H. Jiang, *Phys. Chem. Chem. Phys.*, 2015, **17**, 22872–22881.
42 M. Hu, Y. Jing and X. Zhang, *Phys. Rev. B: Condens. Matter Mater. Phys.*, 2015, **91**, 155408.
43 L. Lindsay and D. Broido, *J. Phys.: Condens. Matter*, 2008, **20**, 165209.
44 X. Wu, V. Varshney, J. Lee, T. Zhang, J. L. Wohlwend, A. K. Roy and T. Luo, *Nano Lett.*, 2016, **16**, 3925–3935.
45 G. Qin, Z. Qin, H. Wang and M. Hu, *Phys. Rev. B*, 2017, **95**, 195416.
46 B. Fultz, *Prog. Mater. Sci.*, 2010, **55**, 247–352.
47 N. Mounet and N. Marzari, *Phys. Rev. B: Condens. Matter Mater. Phys.*, 2005, **71**, 205214.

